ISSN 0915-633X

NATIONAL INSTITUTE FOR FUSION SCIENCE

Clear Detection of Negative Pionlike Particles from H_2 Gas Discharge in Magnetic Field

J. Uramoto

(Received - July 7, 1997)

NIFS-512 Oct. 1997

RESEARCH REPORT
NIFS Series

NAGOYA, JAPAN

Clear detection of negative pionlike particles from H_2 gas discharge in magnetic field

Jōshin URAMOTO

National Institute for Fusion Science
332-6 Orosh-cho, Toki-shi, Gifu, 509-52, Japan

Abstract

Electron density outside H_2 gas discharge plasma along magnetic field, is abruptly reduced as H^- ions are produced. From the region, negative pionlike particles π^- are extracted together with H^- ions. Then, as decay products of the π^-, negative muonlike particles μ^- are also observed with high energy electrons. These particles are clearly detected by a magnetic mass analyzer MA utilizing secondary electrons generated in the beam collector of MA and secondary positive ions within MA. The production mechanism of π^- is explained by interaction between an electron bunch and a positive ion bunch in the outside of the plasma.

Keywords: negative pionlike particle π^-, secondary electron, positive ion

In ordinary plasmas, no strong electrical interactions between electron bunches and positive ion bunches are generated due to charge neutralization between electron space charge and positive ion space charge. But, in the outside region of H_2 gas discharge plasma along magnetic field, the electron density is abruptly reduced in comparison to the positive ion density by the volume produced H^- ions[1,2,3] which absorb the low energy electrons quickly. Therefore, some strong electrical interactions between the electron bunches and the positive ion bunches are expected to produce some elementary particles.

Schematic diagrams of the experimental apparatus are shown in Figs. 1. The apparatus is constructed from a H_2 gas discharge plasma in magnetic fields, three extraction electrodes (with an aperture of 3 mm in diameter) to extract some negatively charged particles and a magnetic mass analyzer (90° deflection-type).

A sheet plasma[4] is produced to generate H^- ions effectively and in wide area. That is, the discharge (cylindrical) plasma flow of about 1 cm in diameter is transformed into a sheet plasma flow of about 3 mm in thickness and about 20 cm in width, while the electron components in the initial discharge plasma are accelerated near 55 eV. The sheet plasma flow enters the electron acceleration anode through the main chamber (50 cm long). A uniform magnetic field of about 50 gauss is applied along the sheet plasma flow in the main chamber where the H_2 gas pressure is about 1.5×10^{-3} Torr. The electron acceleration anode current I_A is 20A. A distance between the sheet plasma center and the first extraction electrode (L) is 7.5 cm. The plasma density in the center of the sheet plasma is about 10^{11}/cc and the electron temperature is about 20 eV. The positive ion density in front of the first extraction electrode is estimated to be about 10^{10}/cc from a positive ion saturation current as H_3^+, while the electron density from the Langmuir probe characteristic is about 10^9/cc and the electron temperature is about 3.0 eV. That is, the electron density in front of the first extraction electrode is reduced near 1/10 of the positive ion density.

The negatively charged particles extracted from the H_2 gas discharge plasma, are injected into the ordinary magnetic mass analyzer (MA) through the slit (3 mm × 1 cm) while each mass of the negatively charged particle is estimated by the following relations: From the analyzing magnetic field B_M where the negative current to the beam collector BC shows a peak, the curvature radius r of the mass analyzer and the extraction (acceleration) voltage V_E, we can estimate the mass m of

the negatively charged particle by,

$$m = \frac{Ze\,(B_M r)^2}{2V_E}$$

$$= \frac{8.8 \times 10^{-2}\, Z\,(B_M r)^2\, m_e}{V_E}, \quad \cdots\cdots (1)$$

where e is the electron charge, B_M is in gauss unit, r is in cm unit, V_E is in volt unit and m_e is the electron mass and Z is the charge number. For the curvature radius $r = 4.3$ cm of this mass analyzer, the Eq. (1) is rewritten by

$$m = \frac{1.63\, Z\, B_M^2}{V_E} m_e. \quad \cdots\cdots (2)$$

In the extraction of negatively charged particles, the first extraction electrode (L) is electrically floated, whose potential V_L is about −10V with respect to the electron acceleration anode. A potential V_M of the second extraction electrode (M) is kept at 300V or 75V. A potential V_E of the final extraction electrode (E) is 800V.

In this experiment, it is noted that the back space of the beam collector is shielded[5] perfectly from the diffusion of positive ions as shown in Fig. 1 (B). The dependences of the negative current I^- to the beam collector on the analyzing magnetic field B_M are shown in Figs. 2 (A) and 2 (B) for the beam collector potential $V_{BC} = 0$V and $V_{BC} = 75$V. Obviously, in a case (1) of Fig. 2 (A) or Fig. 2 (B) at the second extraction electrode potential $V_M = 300$V, a peak of I^- at the analyzing magnetic field $B_M \approx (4.0 \times 240)$ gauss = 960 gauss is corresponding to H^- ion, assuming that $Z = 1$ in Eq. (2). That is, we obtain $m \approx 1880\, m_e$ (near the true mass of $H^- = 1842\, m_e$) as $V_E = 800$V. Then, we find that another main peak of I^- at $B_M \approx (1.54 \times 240)$ gauss ≈ 370 gauss is corresponding to a negative pion, assuming that $Z = 1$ in Eq. (2). That is, we obtain $m \approx 278\, m_e$ (near the true pion mass = 273 m_e) as $V_E = 800$V.

In another case (2) of Fig. 2 (A) or Fig. 2 (B) at $V_M = 75$V, a peak of I^- at $B_M \approx 960$ gauss is also corresponding to H^- ion. Then, we find that another main peak of I^- at $B_M \approx (1.33 \times 240)$

gauss ≈ 320 gauss is corresponding to a negative muon, assuming that Z = 1 in Eq. (2). That is, we obtain $m \approx 209\ m_e$ (near the true muon mass = 207 m_e) as $V_E = 800V$.

A special peak e_H of I^- is observed at $B_M \approx (0.6 \times 240)$ gauss = 144 gauss as seen in Figs. 2 (A) or 2 (B). We consider that this peak e_H is caused by high energy electrons which come directly from the outside of the sheet plasma. Because the e_H peak position of B_M does not depend on the final extraction voltage V_E while the H^-, π^-, μ^- peaks depend exactly on V_E in Eq. (2). The energy eV_H of high energy electron e_H is estimated to be $eV_H \approx 33.8$ keV, if we take $m = m_e$, $V_E = V_H$ and $B_M \approx 144$ gauss at the e_H peak) in Eq. (2).

When a positive potential $V_{BC} = 75V$ is applied to the beam collector BC, their peaks of I^- increase, as seen in Fig. 2 (B), about 1.3 times for H^- ion, about 200 times for π^- or μ^- and about 50 times for e_H. These large apparent increments of negative current peaks under the positive potential $V_{BC} > 0$ of the beam collector BC, may be explained by the following mechanism due to positive ions within the mass analyzer MA and secondary electrons inside BC: The mechanism is shown in Figs. 3 (A) and (B). For $V_{BC} = 0$ of Fig. 3 (A), the negative current I_1^- appears through a closed circuit (H^-, π^-, μ^-, e_H) — BC — MA. Thus, the I_1^- shows a net current of (H^-, π^-, μ^-, e_H). Here, we observe a positive ion current to BC when a deep negative bias voltage ($V_{BC} < -300V$) is given to BC. The positive ions are produced secondarily from the extracting H^- ions. On the other hand, the negative muonlike particle μ^- (decay product of π^- or direct μ^-) inside BC may generate secondary low energy electrons through high energy electrons of the decay process from μ^-. The (back ground) positive ions within MA and the secondary electrons inside BC are shown by + Ion and e_S in Fig. 3 (B). Thus, for $V_{BC} > 0$ of Fig. 3 (B), another closed circuit of negative current I_2^- appears through BC (e_S) — V_{BC} — MA — (+ Ion). A total charge of secondary electrons (e_S) due to μ^- may be extremely larger than that of π^- or μ^-. By the above mechanism, the apparent negative current I_2^- for π^- or μ^- increases abruptly in comparison with the net negative current I_1^-.

Thus, the π^- particles inside the beam collector can generate the large electron current. These processes may be expressed by, according to the elementary particle theories.

$$\pi^- \rightarrow \mu^- + \upsilon_1 \ , \qquad (3)$$

$$\mu^- \rightarrow e_H + \upsilon_2 + \upsilon_3 \ , \quad \text{..... (4)}$$

$$e_H \rightarrow Ne_S \ , \quad \text{..... (5)}$$

where e_H and (υ_1, υ_2, υ_3) are high energy electron and various neutrinos, and where e_S and N are secondary electron and multiplied number inside metal plate (BC).

We consider that secondary electrons due to H^- ions are produced on the surface of BC at only a small rate, and that the apparent current (I_2^-) does not increase particularly for the net H^- ion current (I_1^-).

A flight time of π^- from the final extraction electrode E to the beam collector BC is estimated to be about 8×10^{-8} sec by the flight distance $\overline{E.BC} \approx 8.75$ cm and the π^- velocity $\approx 1.1 \times 10^8$ cm/sec at $V_E = 800V$ acceleration. This flight time is comparable with the typical pion life time 2.6×10^{-8} sec. However, as shown in Figs. 2 (A) and 2 (B), the decay product-like particle μ^- depends greatly on the second extraction electrode voltage V_M. This experimental facts show that the decay products (μ^- and e_H) can be generated also between the first extraction electrode L and the second extraction electrode M, if a local velocity of π^- is reduced by a low voltage of V_M.

When the final extraction voltages V_E are reduced below 500V, the π^- peak of I^- does not appear and only the μ^- peak of I^- appears extractly for V_E in Eq. (2), even if the second extraction voltage V_M is 300V. We consider that the π^- decays into the μ^- as the flight time of π^- much exceeds 10^{-7} sec.

A power source for the net current I_1^- of π^- as shown in Fig. 2 (A), must be considered in the outside of the sheet plasma. To produce one pion, an energy of $E_\pi = 139.6$ MeV or 2.2×10^{-11} Joule is required. Thus, a net current I_π^- of the produced π^- is estimated from an effective power W_{ef} (W) which may be caused by the electron-positive ion bunches interaction in the outside of the sheet plasma. That is, if the kinetic energy of π^- is neglected, the net current I_π^- (μA) is expressed by

$$I_\pi^- = \frac{eW_{ef}}{E_\pi} = 7.1 \times 10^{-3} \ W_{ef} \ (\mu A) \ . \quad \text{..... (6)}$$

Since the net current I_π^- is about 0.01 μA (= I_1^-) from Fig. 2 (A), the effective power W_{ef} must be

about 1 5W from Eq. (6). On the other hand, the electron (or positive ion) density is about 10^9/cc (or 10^{10}/cc) in the outside of the sheet plasma and the extraction area of π^- is about 0.07 cm^2 (for 0.3 cm in diameter). As an estimation, we can obtain $W_{ef} \approx$ 1.5W easily in the extraction area of 0.07 cm^2 if an effective potential and current of about 165V and 9 mA are induced for the electron bunch (~10^9/cc) from the ion bunch. For this physical mechanism of negative pion production, we have proved already[6,7] that negative pionlike particles are produced from a low energy electron beam of (100 eV ~ 1200 eV in a few mA) and it's secondary positive ion beam whose beam-electrons are magnetically (in cyclotron motions) bunched and beam-ions are electrically bunched A schematic diagram[7] for that physical mechanism of the negative pionlike particle production, is shown in Fig. 4, where the positive ion beam is produced secondarily by decelerating the first electron beam and introducing a neutral gas G to produce a plasma region between S and A in Fig. 4.

References

1) J.M. Wadehra: *Appl. Phys. Lett.* **35** (1979) 917.

2) M. Bacal and G.W. Hamilton: *Phys. Rev. Lett.* **42** (1979) 1538.

3) M. Allan and S.F. Wong: *Phys. Rev. Lett.* **41** (1978) 1971.

4) J. Uramoto: Journal of the vacuum society of Japan, **27** (1984) 610 in Japanese.

5) J. Uramoto: National Institute of Fusion Science, Nagoya, Japan-Research Report, NIFS-400 (1996).

6) J. Uramoto: NIFS-277 (1994).

7) J. Uramoto: NIFS-414 (1996).

Figure Captions

Fig. 1 (A) Schematic diagram of experimental apparatus.

1: Cylindrical plasma in discharge anode 2: Discharge cathode. 3 H_2 gas flow. 4: Discharge power supply. 5: Electron acceleration power supply. 6: Vacuum pump. 7: Area where cylindrical plasma is transformed into sheet plasma 8: Insulation tube. 9: A pair of permanent magnets 10: Magnetic field coils. 11: Electron acceleration anode. I_A: Current to electron acceleration anode. CP: Cylindrical plasma. SP: Sheet plasma B_Z: Magnetic field. L: First extraction electrode. M: Second extraction electrode E: Final extraction electrode. V_M: Potential (variable) of second extraction electrode with respect to electron acceleration anode. V_E: Potential (800V) of final extraction electrode with respect to electron acceleration anode. MA: Magnetic deflection (90°) mass analyzer B_M: Magnetic field intensity of MA. BC: Beam collector of MA. V_{BC}: Positive potential of BC with respect to MA. I^-: Negative current to BC. H_0^-: Hydrogen negative ions outside of sheet plasma. H^-: Accelerated hydrogen negative ions. π_0^-: Negative pionlike particles outside of sheet plasma. π^-: Accelerated negative pionlike particles.

Fig. 1 (B) Schematic diagram of mass analyzer.

S: Entrance slit position. X: Entrance of uniform magnetic field.

Ins: Insulator behind BC. + Ion: Positive ions in front of BC. Fe: shows Iron.

(See Fig. 4 as resemblance mechanism).

Fig. 2 (A) Dependences of negative current I^- to BC on magnetic field intensity B_M of MA under beam collector potential $V_{BC} = 0V$.

(1): Potential of second extraction electrode $V_M = 300V$. (2): $V_M = 75V$. H^-: Peak of I^- corresponding to hydrogen negative ion. π^-: Peak of I^- corresponding to negative pionlike particle. μ^-: Peak of I^- corresponding to negative muonlike particle. e_H: peak of I^- corresponding to high energy electron.

Fig. 2 (B) Dependence of I^- to BC on B_M of MA under $V_{BC} = 75V$.

(1): $V_M = 300V$. (2): $V_M = 75V$. H^-, π^-, μ^-, e_H: See captions of Fig. 2 (A).

Fig. 3 (A) Closed circuit of negative charged particle current under $V_{BC} = 0V$.

I_1^-: Net current of negative charged particle. (H^-, π^-, μ^-, e_H): See captions of Fig. 2 (A). BC: Beam collector. MA: Magnetic mass analyzer.

Fig. 3 (B) Increment circuit of negative current under $V_{BC} > 0$.

+Ion: Positive ions within MA. e_S: secondary electrons inside BC. I_2^-: Increased negative current.

Fig. 4 A schematic diagram as a physical mechanism.

F: Filament as electron emitter. K: Cathode of electron gun. A: Anode of electron gun. V_A: Initial electron acceleration voltage. I_A: Total negative current. F.E.B.: First electron beam. G: Neutral gas. D: Decelerator of F.E.B. S: Entrance slit. Ins: Insulator. I.B.: Ion beam. S.E.B.: Second electron beam. e: Electrons with cyclotron motions. μ^-: Negative muonlike particle. (MA): Magnetic mass analyzer. Fe: Iron. C: Magnetic Coil. (N): North pole of electro-magnet. (S): South pole. B_M: Analyzing magnetic field. BC: Beam collector. I^-: Negative current to BC. V_S: Bias voltage of BC with respect to mass analyzer body. i: Ion bunch. π^-: Negative pionlike particle. Ins: Insulator.

Appendix

As shown in Figs. A1 (A) and A1 (B), if the back metal plate (BMP) of the magnetic mass analyzer MA (of Fig. 1 (B) in this paper) is arranged, H^+ ions will be generated secondarily within MA by the H^- ion beam arriving to BMP. This fact is confirmed from a current characteristic to the beam collector BC of MA under a deep negative bias voltage $V_{BC} < 0$. A dependence of the current to BC on the mass analyzing magnetic field B_M is shown in Fig. A2 under $V_{BC} = -300V$. Obviously, positive currents I^+ are observed for $B_M < 3.0 \times 240$ gauss while a peak of I^+ appears near $B_M \approx 1.3 \times 240$ gauss corresponding to the arrival of the muonlike particle beam on BC.

Next, as shown in Figs. A3 (A) and A3 (B), if the back metal plate (BMP) is removed, the H^+ ions will be reduced abruptly. This fact is confirmed also from current characteristics to BC under various BC bias voltages. Dependences of the current to BC on B_M are shown in Figs. A4 (A) and A4 (B) under $V_{BC} = -300V$ and $V_{BC} = 75V$. It should be noted that negative current peaks corresponding to the high energy electron (e_H) and the negative muonlike particle (μ^-) appear even if the deep negative bias voltage is applied to BC. Moreover, even if the positive bias voltage ($V_{BC} = 75V$) is applied to BC, the increased negative current peak as seen in Fig. 2 (B) of this paper, dose not appear. That is, if the positive ions (H^+) does not exist around the beam collector BC, the large increment of the negative peak current corresponding to the negative muonlike particle does not occur.

Results in this Appendix are the same also for the pionlike particle under the second extraction voltage $V_M = 300V$.

Figure Captions of Appendix

Fig. A1 Schematic diagram of mass analyzer (MA) with BMP.

BMP: Back metal plate. E: Final extraction electrode. V_E: Applied voltage of E (800V). M: Second extraction electrode (V_M = 75V). L: First extraction electrode (V_L = −10V). Fe: Shows Iron. C: Magnetic coil. (N): North pole of electro-magnetic. (S): South pole. B_M: Analyzing magnetic field of MA. BC: Beam collector of MA. V_{BC}: Potential of BC with respect to MA. Ins: Insulator behind BC. I: Current to BC. S: Entrance slit position. X: Entrance of uniform magnetic field (B_M). π_0^-: Negative pionlike particle outside of sheet plasma. π^-: Accelerated negative pionlike particle. H_0^-: Hydrogen negative ions outside of sheet plasma. H^-: Accelerated hydrogen negative ions. H^+: Hydrogen positive ions generated secondarily from H^- ions.

Fig. A2 Dependence of current to BC on B_M under V_{BC} = −300V in a case with BMP.

(B_M: Analyzing magnetic field of mass analyzer MA). (BMP: Back metal plate within MA). (V_{BC}: Bias voltage of beam collector BC). I^+: Positive current to BC. I^-: Negative current to BC. H^-: Hydrogen negative ion. (μ^-): Show a positive ion peak corresponding negative muonlike particle decayed from negative pionlike particle π^-.

Fig. A3 Schematic diagram for mass analyzer (MA) without BMP.

See captions of Fig. A1.

Fig. A4 (A) Dependence of current to BC on B_M under V_{BC} = −300V in a case without BMP.

e_H: High energy electron from outside of sheet plasma. (See caption of Fig. A2).

Fig. A4 (B) Dependence of current to BC on B_M under V_{BC} = 75V in a case without BMP.

e_H: High energy electron. (See caption of Fig. A2).

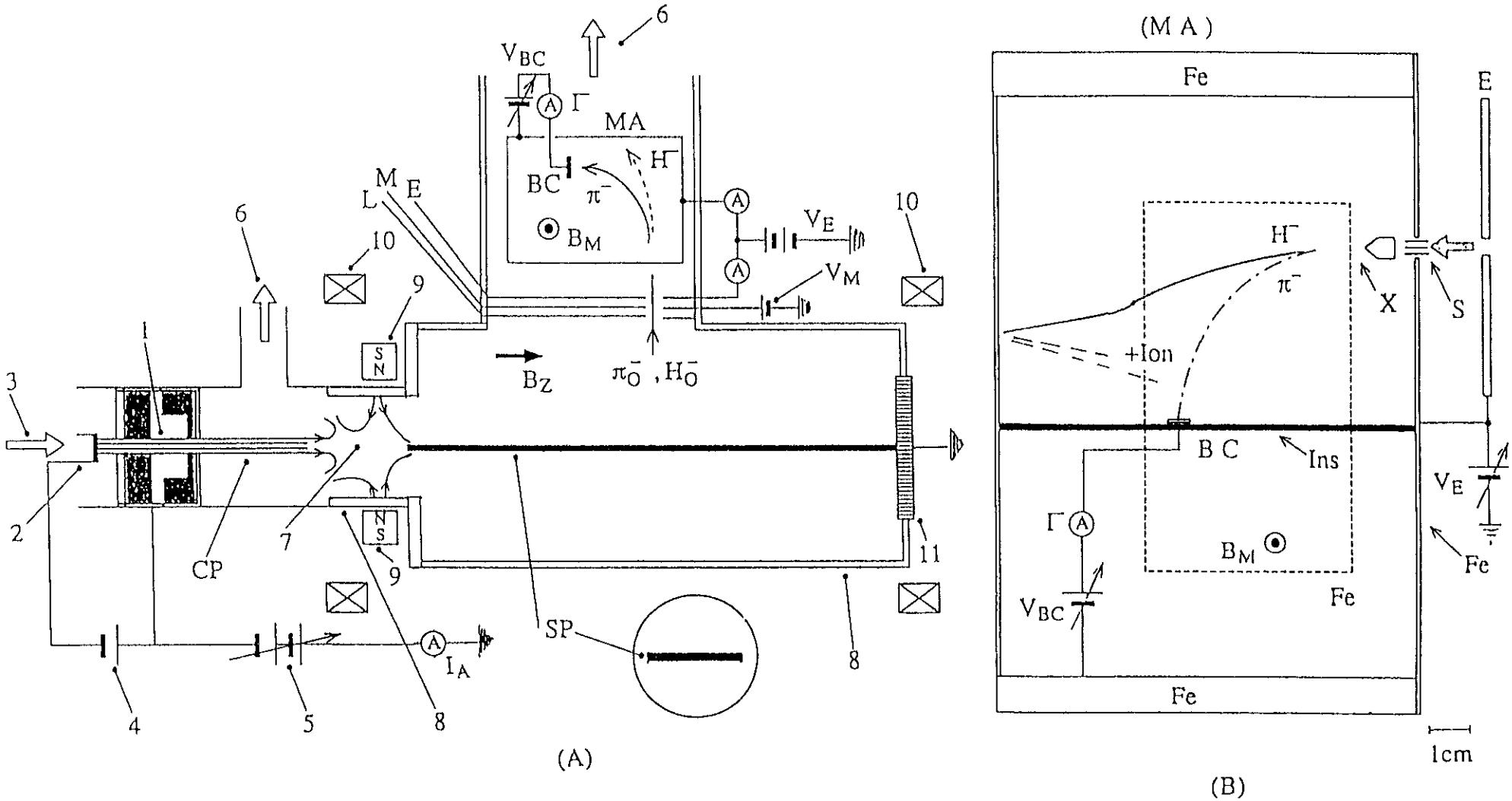
6
V_{BC}
Γ
MA
BC
H^-
π^-
B_M
M
L
E
V_E
V_M
10
9
1
3
2
CP
7
B_Z
π_O^- , H_O^-
11
SP
8
I_A
4
5
(A)
(M A)
Fe
E
X
S
+Ion
B C
Ins
V_E
Fe
B_M
V_{BC}
1cm
(B)

Fig. 1

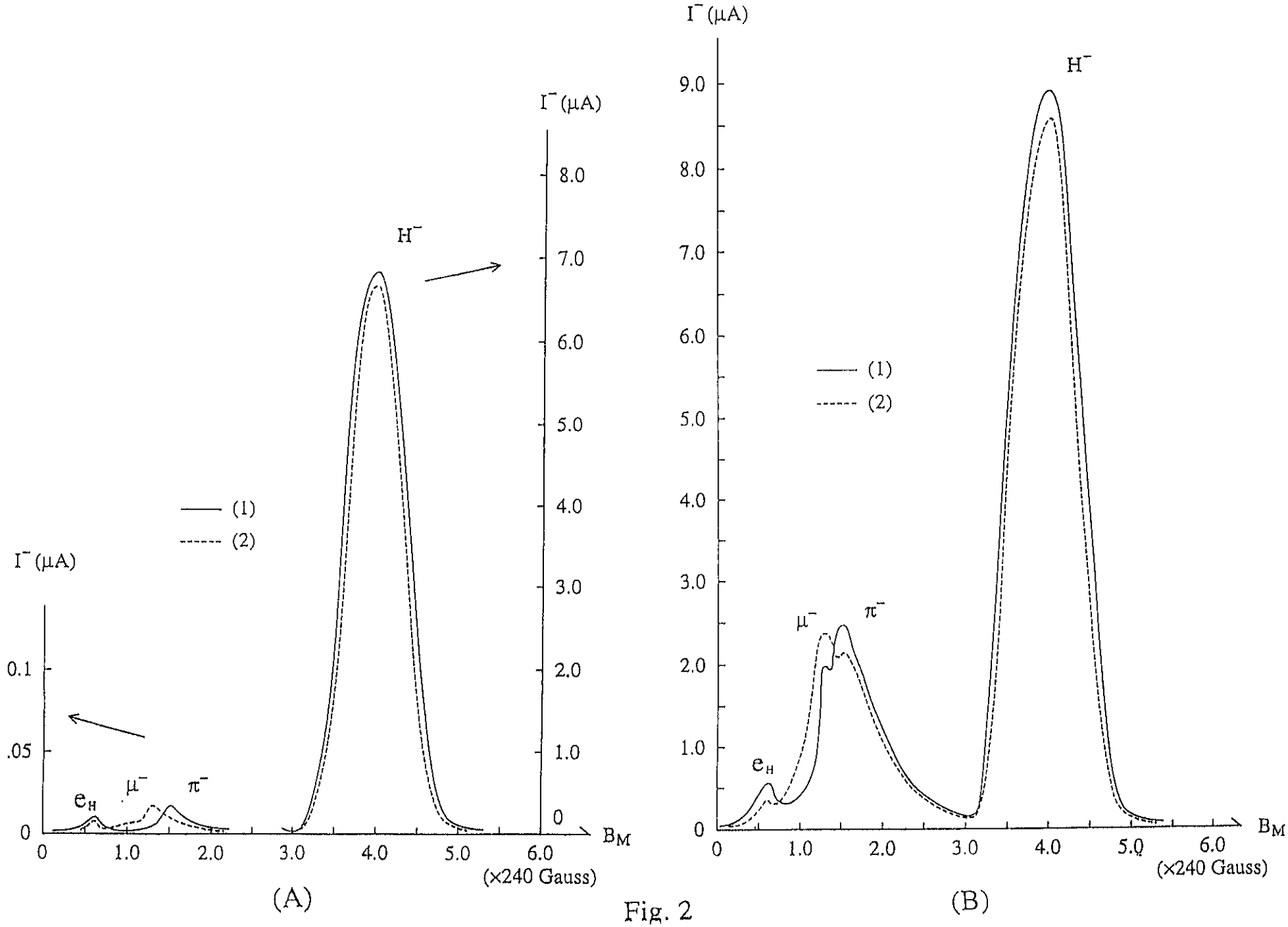
I⁻ (μA)
H⁻
(1)
(2)
I⁻ (μA)
0.1
.05
0
e_H
μ⁻
π⁻
0
1.0
2.0
3.0
4.0
5.0
6.0
B_M
(×240 Gauss)
(A)
I⁻ (μA)
H⁻
9.0
8.0
7.0
6.0
5.0
4.0
3.0
2.0
1.0
0
(1)
(2)
μ⁻
π⁻
e_H
0
1.0
2.0
3.0
4.0
5.0
6.0
B_M
(×240 Gauss)
(B)

Fig. 2

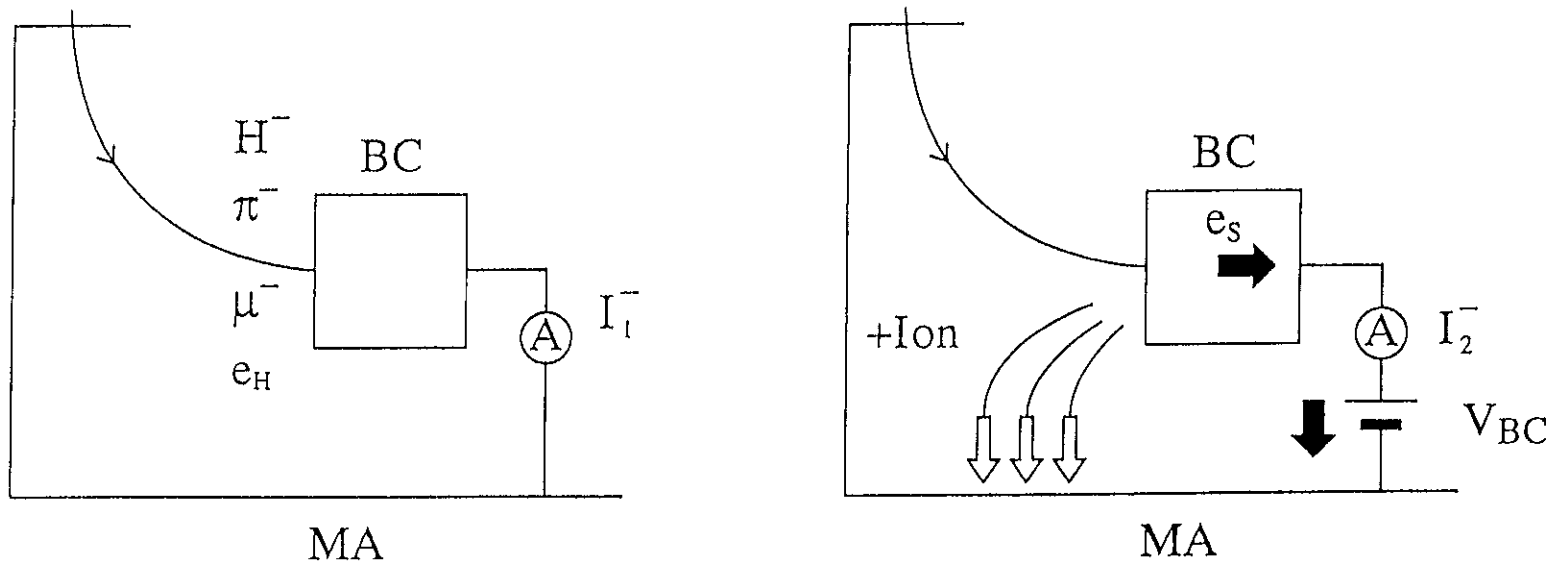

(A) (B)

Fig. 3

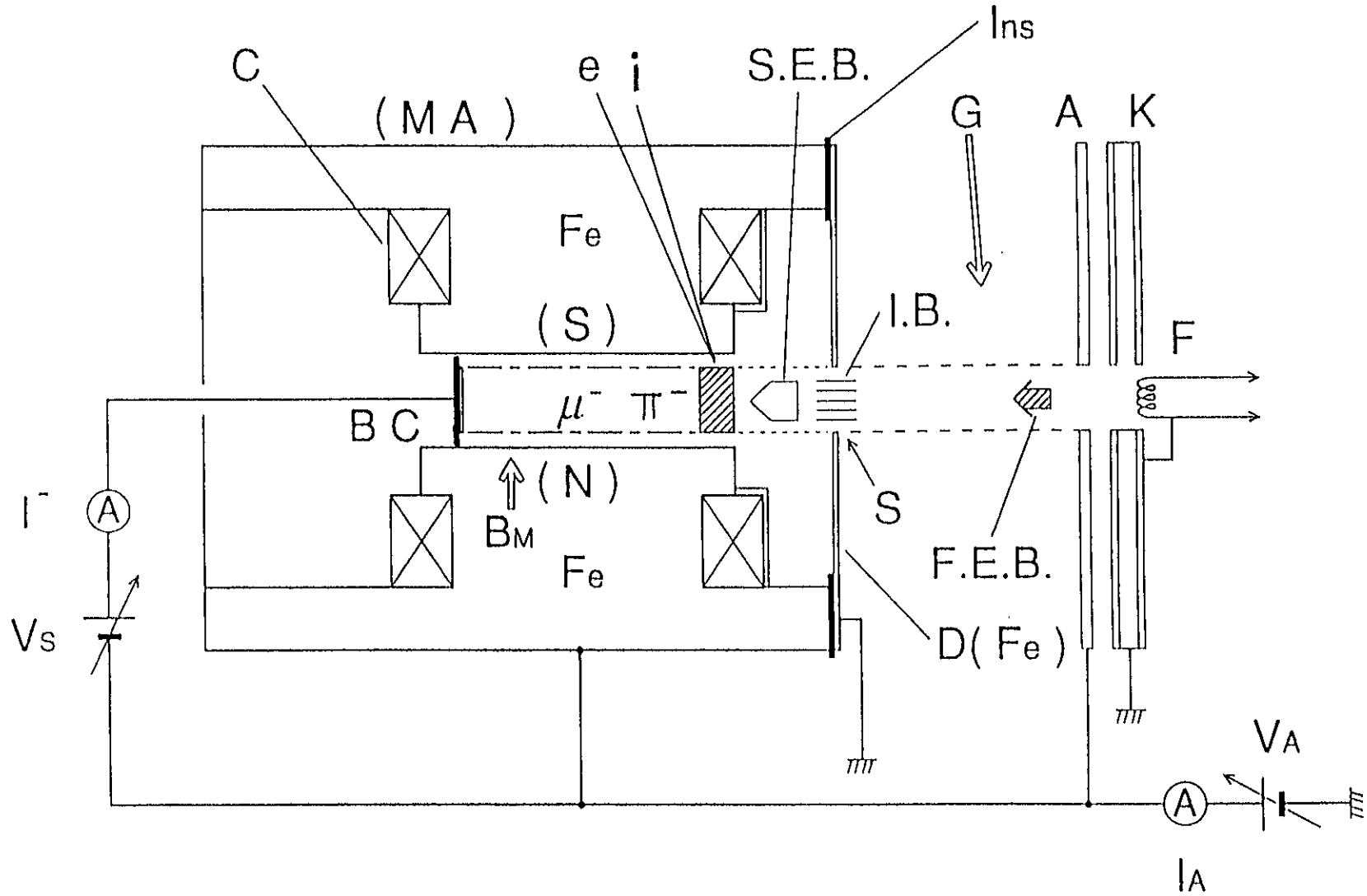

Fig. 4

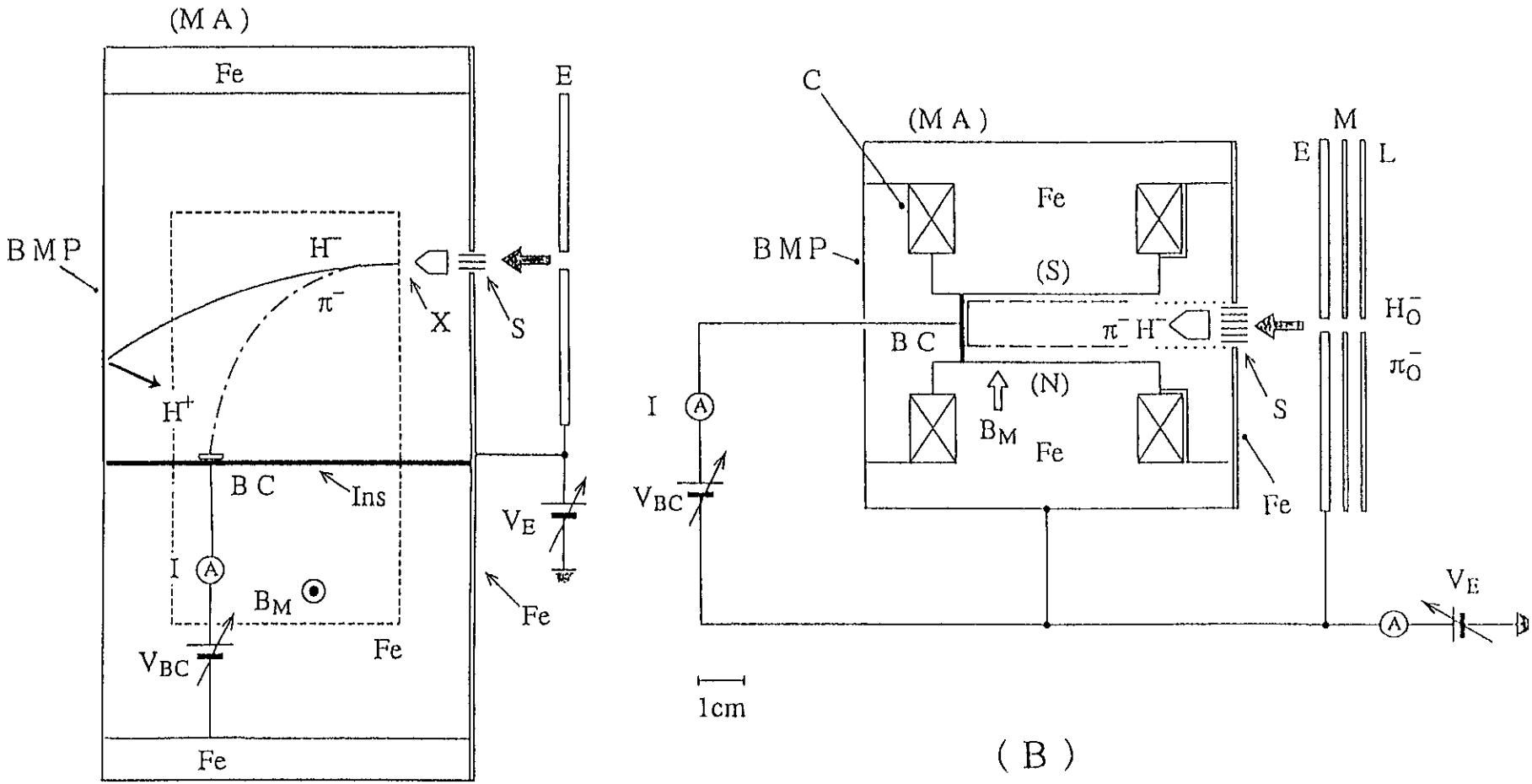
(M A)
Fe
E
BMP
H⁻
π⁻
X
S
H⁺
B C
Ins
I
A
BM
VBC
Fe
VE
Fe
Fe
C
(M A)
M
E
L
Fe
BMP
(S)
H⁻O
π⁻O
π⁻ H⁻
B C
(N)
I
A
BM
Fe
S
VBC
Fe
VE
A
1cm
(A)
(B)

Fig. A1

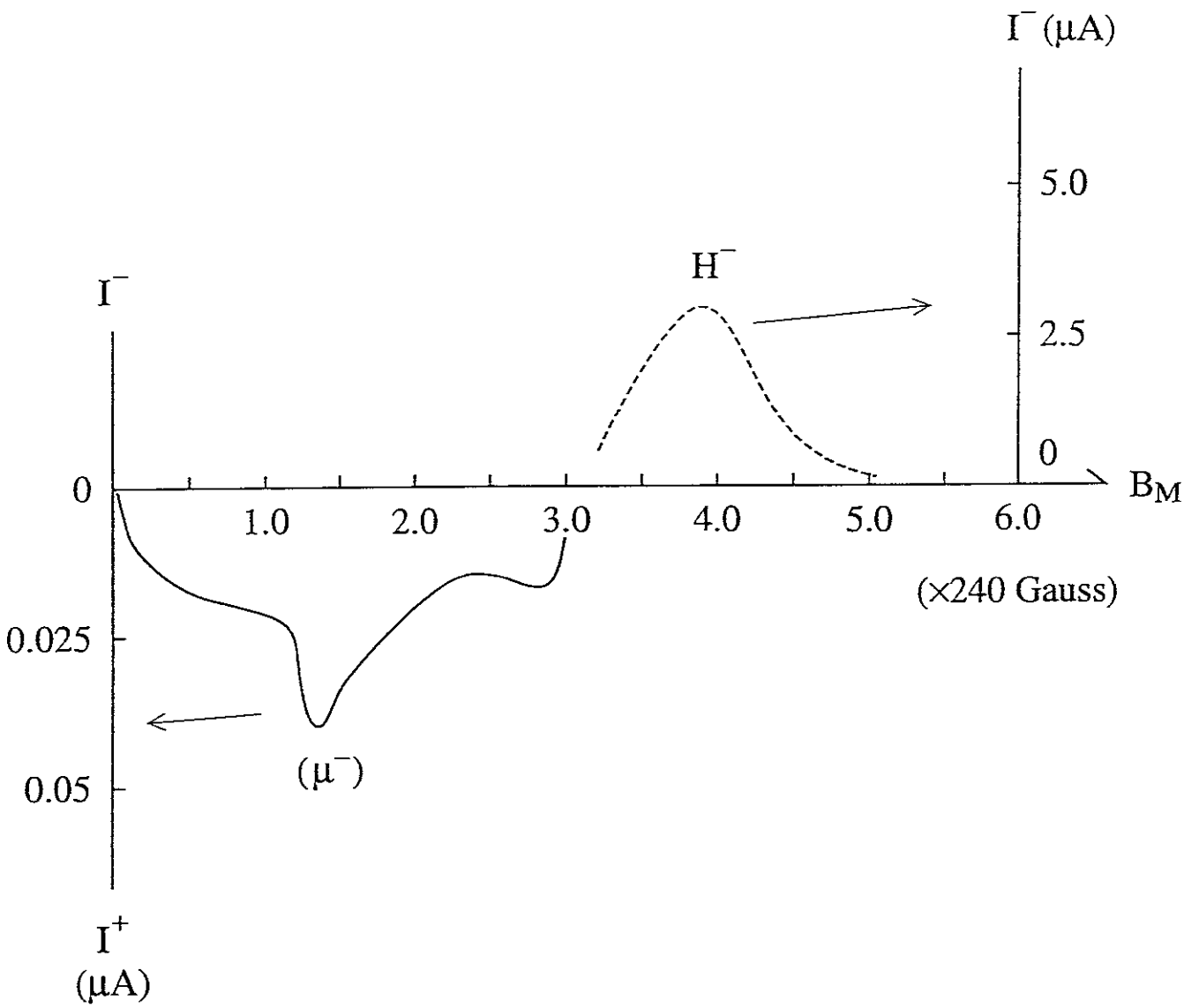

Fig. A2

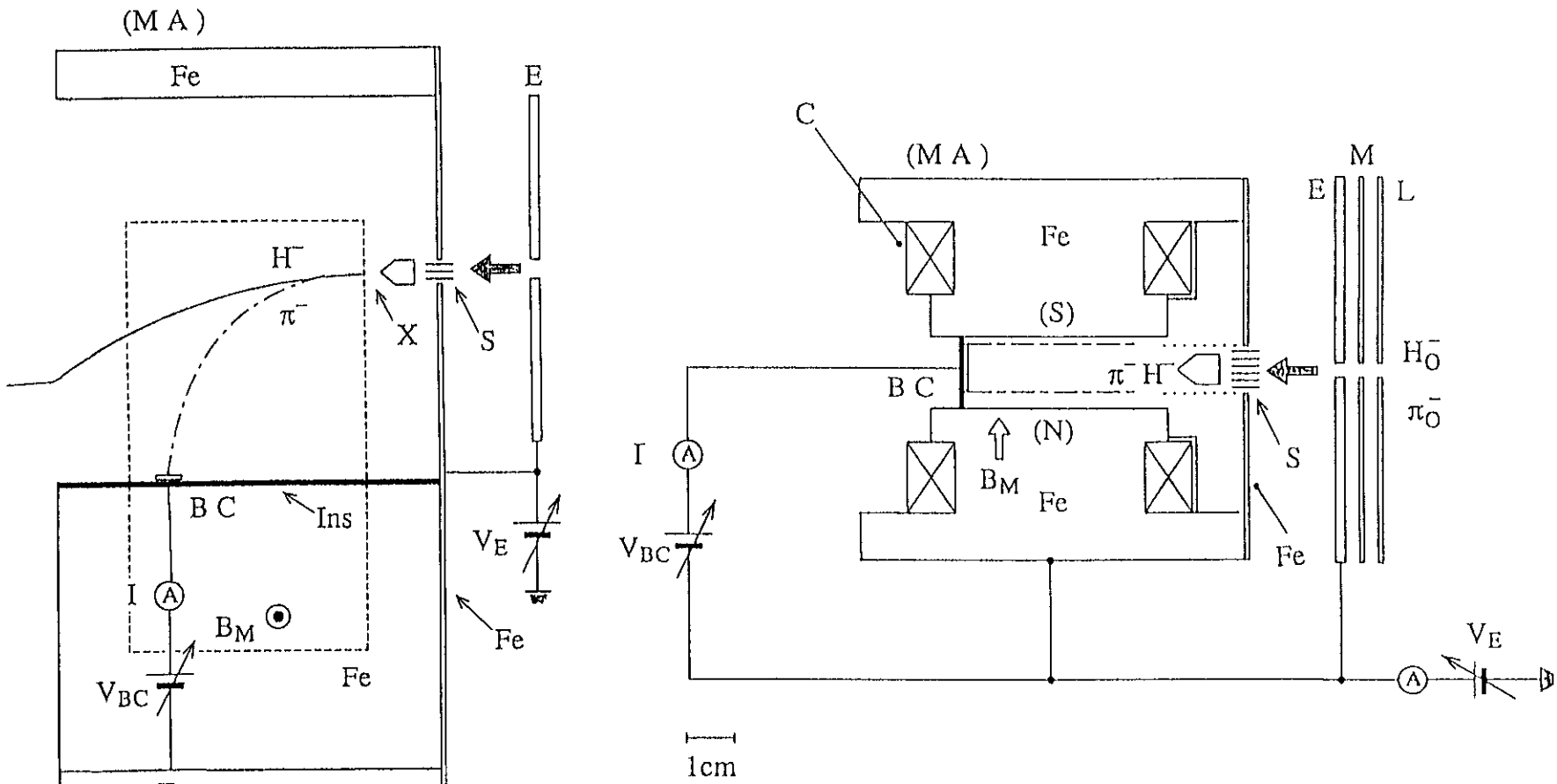
(M A)
Fe
E
H⁻
π⁻
X
S
B C
Ins
I
A
B_M
V_BC
Fe
V_E
Fe
Fe
C
(M A)
Fe
(S)
B C
π⁻ H⁻
(N)
B_M
Fe
I
A
V_BC
S
Fe
M
E
L
H⁻_O
π⁻_O
V_E
A
1cm

(A)

(B)

Fig. A3

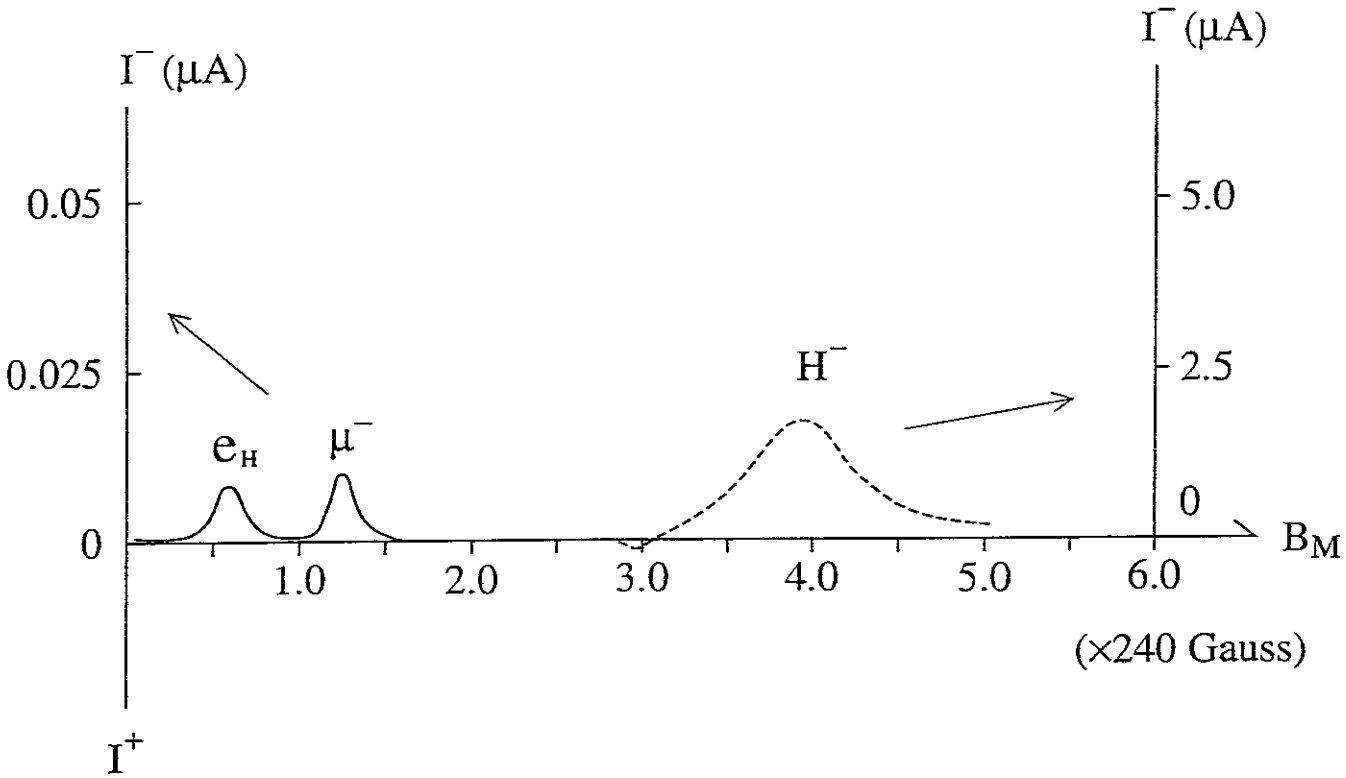

Fig. A4 (A)

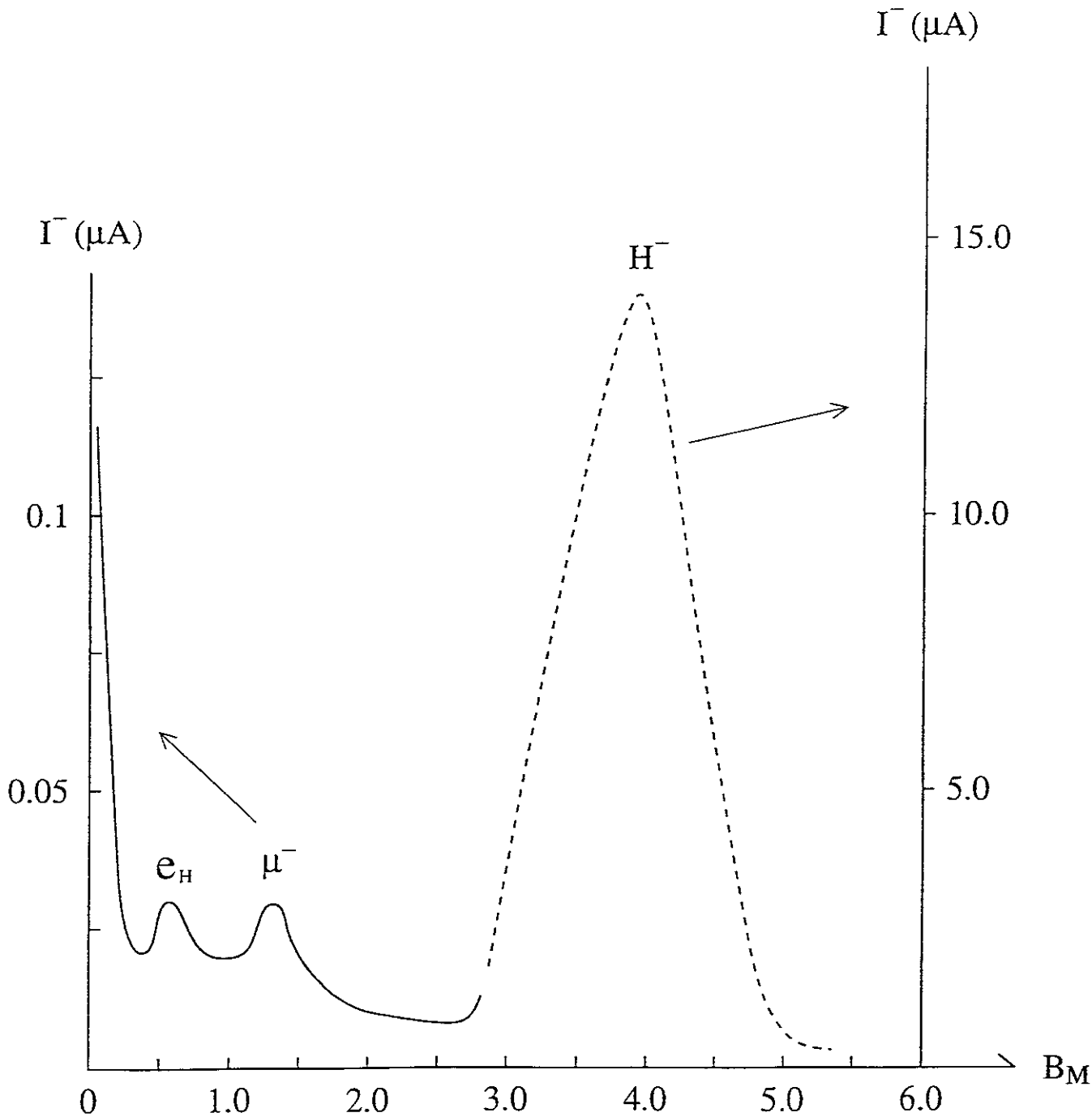

Fig. A4 (B)

(×240 Gauss)

Recent Issues of NIFS Series

NIFS-465 V.S. Voitsenya, S. Masuzaki, O. Motojima, N. Noda and N. Ohyabu,
On the Use of CX Atom Analyzer for Study Characteristics of Ion Component in a LHD Divertor Plasma; Dec. 1996

NIFS-466 H. Miura and S. Kida,
Identification of Tubular Vortices in Complex Flows; Dec. 1996

NIFS-467 Y. Takeiri, Y. Oka, M. Osakabe, K. Tsumori, O. Kaneko, T. Takanashi, E. Asano, T. Kawamoto, R. Akiyama and T. Kuroda,
Suppression of Accelerated Electrons in a High-current Large Negative Ion Source; Dec. 1996

NIFS-468 A. Sagara, Y. Hasegawa, K. Tsuzuki, N. Inoue, H. Suzuki, T. Morisaki, N. Noda, O. Motojima, S. Okamura, K. Matsuoka, R. Akiyama, K. Ida, H. Idei, K. Iwasaki, S. Kubo, T. Minami, S. Morita, K. Narihara, T. Ozaki, K. Sato. C. Takahashi, K. Tanaka, K. Toi and I. Yamada,
Real Time Boronization Experiments in CHS and Scaling for LHD; Dec. 1996

NIFS-469 V.L. Vdovin, T.Watari and A. Fukuyama,
3D Maxwell-Vlasov Boundary Value Problem Solution in Stellarator Geometry in Ion Cyclotron Frequency Range (final report); Dec. 1996

NIFS-470 N. Nakajima, M. Yokoyama, M. Okamoto and J. Nührenberg,
Optimization of M=2 Stellarator; Dec. 1996

NIFS-471 A. Fujisawa, H. Iguchi, S. Lee and Y. Hamada,
Effects of Horizontal Injection Angle Displacements on Energy Measurements with Parallel Plate Energy Analyzer; Dec. 1996

NIFS-472 R. Kanno, N. Nakajima, H. Sugama, M. Okamoto and Y. Ogawa,
Effects of Finite-β and Radial Electric Fields on Neoclassical Transport in the Large Helical Device; Jan. 1997

NIFS-473 S. Murakami, N. Nakajima, U. Gasparino and M. Okamoto,
Simulation Study of Radial Electric Field in CHS and LHD; Jan. 1997

NIFS-474 K. Ohkubo, S. Kubo, H. Idei, M. Sato, T. Shimozuma and Y. Takita,
Coupling of Tilting Gaussian Beam with Hybrid Mode in the Corrugated Waveguide; Jan. 1997

NIFS-475 A. Fujisawa, H. Iguchi, S. Lee and Y. Hamada,
Consideration of Fluctuation in Secondary Beam Intensity of Heavy Ion Beam Prove Measurements; Jan. 1997

NIFS-476 Y. Takeiri, M. Osakabe, Y. Oka, K. Tsumori, O. Kaneko, T. Takanashi, E. Asano, T. Kawamoto, R. Akiyama and T. Kuroda,

Long-pulse Operation of a Cesium-Seeded High-Current Large Negative Ion Source; Jan. 1997

NIFS-477 H. Kuramoto, K. Toi, N. Haraki, K. Sato, J. Xu, A. Ejiri, K. Narihara, T. Seki, S. Ohdachi, K. Adati, R. Akiyama, Y. Hamada, S. Hirokura, K. Kawahata and M. Kojima,
Study of Toroidal Current Penetration during Current Ramp in JIPP T-IIU with Fast Response Zeeman Polarimeter; Jan., 1997

NIFS-478 H. Sugama and W. Horton,
Neoclassical Electron and Ion Transport in Toroidally Rotating Plasmas; Jan. 1997

NIFS-479 V.L. Vdovin and I.V. Kamenskij,
3D Electromagnetic Theory of ICRF Multi Port Multi Loop Antenna; Jan. 1997

NIFS-480 W.X. Wang, M. Okamoto, N. Nakajima, S Murakami and N. Ohyabu,
Cooling Effect of Secondary Electrons in the High Temperature Divertor Operation; Feb. 1997

NIFS-481 K. Itoh, S.-I. Itoh, H. Soltwisch and H.R. Koslowski,
Generation of Toroidal Current Sheet at Sawtooth Crash; Feb. 1997

NIFS-482 K. Ichiguchi,
Collisionality Dependence of Mercier Stability in LHD Equilibria with Bootstrap Currents; Feb. 1997

NIFS-483 S. Fujiwara and T. Sato,
Molecular Dynamics Simulations of Structural Formation of a Single Polymer Chain: Bond-orientational Order and Conformational Defects; Feb. 1997

NIFS-484 T. Ohkawa,
Reduction of Turbulence by Sheared Toroidal Flow on a Flux Surface; Feb. 1997

NIFS-485 K. Narihara, K. Toi, Y. Hamada, K. Yamauchi, K. Adachi, I. Yamada, K. N. Sato, K. Kawahata, A. Nishizawa, S. Ohdachi, K. Sato, T. Seki, T. Watari, J. Xu, A. Ejiri, S. Hirokura, K. Ida, Y. Kawasumi, M. Kojima, H. Sakakita, T. Ido, K. Kitachi, J. Koog and H. Kuramoto,
Observation of Dusts by Laser Scattering Method in theJIPPT-IIU Tokamak Mar. 1997

NIFS-486 S. Bazdenkov, T. Sato and The Complexity Simulation Group,
Topological Transformations in Isolated Straight Magnetic Flux Tube; Mar. 1997

NIFS-487 M. Okamoto,
Configuration Studies of LHD Plasmas; Mar. 1997

NIFS-488 A. Fujisawa, H. Iguchi, H. Sanuki, K. Itoh, S. Lee, Y. Hamada, S. Kubo, H. Idei, R. Akiyama, K. Tanaka, T. Minami. K. Ida. S. Nishimura, S. Morita, M. Kojima, S. Hidekuma, S.-I. Itoh, C. Takahashi. N. Inoue, H. Suzuki, S. Okamura and K. Matsuoka,
Dynamic Behavior of Potential in the Plasma Core of the CHS Heliotron/Torsatron; Apr. 1997

NIFS-489 T. Ohkawa,
Pfirsch - Schlüter Diffusion with Anisotropic and Nonuniform Superthermal Ion Pressure; Apr. 1997

NIFS-490 S. Ishiguro and The Complexity Simulation Group,
Formation of Wave-front Pattern Accompanied by Current-driven Electrostatic Ion-cyclotron Instabilities; Apr. 1997

NIFS-491 A. Ejiri, K. Shinohara and K. Kawahata,
An Algorithm to Remove Fringe Jumps and its Application to Microwave Reflectometry; Apr. 1997

NIFS-492 K. Ichiguchi, N. Nakajima, M. Okamoto,
Bootstrap Current in the Large Helical Device with Unbalanced Helical Coil Currents; Apr. 1997

NIFS-493 S. Ishiguro, T. Sato, H. Takamaru and The Complexity Simulation Group,
V-shaped dc Potential Structure Caused by Current-driven Electrostatic Ion-cyclotron Instability; May 1997

NIFS-494 K. Nishimura, R. Horiuchi, T. Sato,
Tilt Stabilization by Energetic Ions Crossing Magnetic Separatrix in Field-Reversed Configuration; June 1997

NIFS-495 T. -H. Watanabe and T. Sato,
Magnetohydrodynamic Approach to the Feedback Instability; July 1997

NIFS-496 K. Itoh, T. Ohkawa, S. -I.Itoh, M. Yagi and A. Fukuyama
Suppression of Plasma Turbulence by Asymmetric Superthermal Ions; July 1997

NIFS-497 T. Takahashi, Y. Tomita, H. Momota and Nikita V. Shabrov,
Collisionless Pitch Angle Scattering of Plasma Ions at the Edge Region of an FRC; July 1997

NIFS-498 M. Tanaka, A.Yu Grosberg, V.S. Pande and T. Tanaka,
Molecular Dynamics and Structure Organization in Strongly-Coupled Chain of Charged Particles; July 1997

NIFS-499 S. Goto and S. Kida,
Direct-interaction Approximation and Reynolds-number Reversed Expansion for a Dynamical System; July 1997

NIFS-500 K. Tsuzuki, N. Inoue, A. Sagara, N. Noda, O. Motojima, T. Mochizuki, T. Hino and T.

Yamashina,
Dynamic Behavior of Hydrogen Atoms with a Boronized Wall; July 1997

NIFS-501 I. Viniar and S. Sudo,
Multibarrel Repetitive Injector with a Porous Pellet Formation Unit; July 1997

NIFS-502 V. Vdovin, T. Watari and A. Fukuyama,
An Option of ICRF Ion Heating Scenario in Large Helical Device; July 1997

NIFS-503 E. Segre and S. Kida,
Late States of Incompressible 2D Decaying Vorticity Fields; Aug. 1997

NIFS-504 S. Fujiwara and T. Sato,
Molecular Dynamics Simulation of Structural Formation of Short Polymer Chains; Aug. 1997

NIFS-505 S. Bazdenkov and T. Sato
Low-Dimensional Model of Resistive Interchange Convection in Magnetized Plasmas; Sep. 1997

NIFS-506 H. Kitauchi and S. Kida,
Intensification of Magnetic Field by Concentrate-and-Stretch of Magnetic Flux Lines; Sep. 1997

NIFS-507 R.L. Dewar,
Reduced form of MHD Lagrangian for Ballooning Modes; Sep. 1997

NIFS-508 Y.-N. Nejoh,
Dynamics of the Dust Charging on Electrostatic Waves in a Dusty Plasma with Trapped Electrons; Sep.1997

NIFS-509 E. Matsunaga, T.Yabe and M. Tajima,
Baroclinic Vortex Generation by a Comet Shoemaker-Levy 9 Impact; Sep. 1997

NIFS-510 C.C. Hegna and N. Nakajima,
On the Stability of Mercier and Ballooning Modes in Stellarator Configurations; Oct. 1997

NIFS-511 K. Orito and T. Hatori,
Rotation and Oscillation of Nonlinear Dipole Vortex in the Drift-Unstable Plasma; Oct. 1997

NIFS-512 J. Uramoto,
Clear Detection of Negative Pionlike Particles from H_2 Gas Discharge in Magnetic Field; Oct. 1997